

Resonant two-magnon Raman scattering in antiferromagnetic insulators

Andrey V. Chubukov

*Department of Physics, University of Wisconsin-Madison, 1150 University ave., Madison, WI
53706*

and P.L. Kapitza Institute for Physical Problems, Moscow, Russia

David M. Frenkel

Texas Center for Superconductivity, University of Houston, Houston, TX 77204-5932
and Department of Physics, Science and Technology Center for Superconductivity,
University of Illinois at Urbana-Champaign, 1110 West Green Street, Urbana, IL 61801*

(today)

Abstract

We propose a theory of two-magnon *resonant* Raman scattering from antiferromagnetic insulators, which contains information both on the magnetism and the carrier properties in the lightly doped phases. We argue that the conventional theory does not work in the resonant regime, in which the energy of the incident photon is close to the gap between the conduction and valence bands. We identify the diagram which gives the dominant contribution to Raman intensity in this regime and show that it can explain the unusual features in the two-magnon profile and in the two-magnon peak intensity dependence on the incoming photon frequency.

There is a widespread belief that strong electron-electron correlations in the high- T_c compounds may hold a clue to the phenomenon of high-temperature superconductivity [1]. One of the manifestations of these correlations is the fact that the insulating parent compounds are antiferromagnets. An important probe of antiferromagnetism is magnetic Raman scattering [2,3]. Its prominent signature in the underdoped high- T_c materials is a strong peak observed at about 3000cm^{-1} . To first approximation, this peak can be attributed to inelastic scattering from the two-magnon excitations [3–5].

The traditional framework for understanding the two-magnon Raman scattering in antiferromagnets has been an effective Hamiltonian for the interaction of light with spin degrees of freedom known as the Loudon-Fleury Hamiltonian [6], $H = \alpha \sum_{\langle ij \rangle} (\hat{\mathbf{e}}_i \cdot \mathbf{R}_{ij})(\hat{\mathbf{e}}_f \cdot \mathbf{R}_{ij}) \mathbf{S}_i \cdot \mathbf{S}_j$, where $\hat{\mathbf{e}}_i$ and $\hat{\mathbf{e}}_f$ are the polarization vectors of the in- and outgoing photons, α is the coupling constant, and \mathbf{R}_{ij} is the vector connecting two nearest neighbor sites i and j . Shastry and Shraiman [7] have recently derived this Hamiltonian starting from the large- U Hubbard model. Working in a localized basis, they performed a hopping expansion controlled by $t/(U - \omega)$, where t and U are the nearest-neighbor hopping and on-site Coulomb repulsion, and ω is of the order of the photon frequencies. The leading term in the expansion turned out to be the Loudon-Fleury Hamiltonian.

This theory works well when the frequencies of the incoming and outgoing photons are considerably smaller than the gap between the conduction and valence bands, which is roughly $2eV$. The experimental reality in high- T_c materials is such, however, that the two-magnon scattering is measured mostly in the resonant regime, when the frequencies of the ingoing and/or outgoing photons are close to the gap value and the cross-sections vary strongly as the incident photon frequency is varied [8,9]. Luckily, it is in this regime that the cross-sections sensitively depend not just on magnetic, but on the carrier properties as well, and this makes understanding the data particularly important.

The profile of the Raman cross-section as a function of the *transferred* photon frequency and the behavior of the two-magnon peak height as a function of the *incident* photon frequency are shown in Fig. 1.

The key experimental features that require explanation are: (a) the two-magnon peak is asymmetric, with the spectral weight shifted to higher frequencies; (b) the Loudon-Fleury Hamiltonian predicts no scattering in the A_{1g} configuration, whereas experimentally the resonant A_{1g} cross-section is about half of that in the B_{1g} geometry; (c) there is only one peak in Fig. 1b — ordinarily one might expect two peaks, the so called ingoing and outgoing resonances [10,11]; (d) a comparison with the dielectric constant shows that the strength of the two-magnon Raman scattering in Fig. 1b is at its maximum away from the band edge, in fact right at the upper end of the features in the optical data that can be interpreted as the particle-hole excitations between the lower and upper Hubbard bands.

In this paper we develop a diagrammatic approach to Raman scattering valid in both nonresonant and resonant regimes. For small frequencies, our results are identical to those of Shastry and Shraiman. However, for $|\omega - U| \sim \mathcal{O}(J)$, we find that the dominant contribution to Raman scattering comes from a diagram which is subleading in the nonresonant region. We will argue that this diagram accounts for most of the experimental features in Fig. 1.

We start with the one-band Hubbard model with $H = -t \sum_{\langle i,j \rangle} (c_{i,\sigma}^\dagger c_{j,\sigma} + h.c) + U \sum_i n_{i\uparrow} n_{i\downarrow}$. In the presence of the slowly varying vector potential $\mathbf{A}(\mathbf{x}, t)$ the Hubbard Hamiltonian gets transformed to

$$H = H^{\mathbf{A}=0} - \frac{e}{\hbar c} \sum \mathbf{j}_q \cdot \mathbf{A}_q + O(\mathbf{A}^2), \quad (1)$$

where $j_q^\alpha = \sum_k \frac{\partial \epsilon_k}{\partial k_\alpha} c_{k+q/2,\sigma}^\dagger c_{k-q/2,\sigma}$ is the current operator, and $\epsilon_k = -2t(\cos k_x + \cos k_y)$ is the electron dispersion. The resonant part of the scattering matrix element M_R is obtained from the term linear in \mathbf{A} in the 2nd order of perturbation theory [10]. In this process, a photon with energy ω_i and momentum which can be safely set equal to zero, creates a virtual particle-hole state of the fermionic system which can emit or absorb two spin-waves with momenta \mathbf{k} and $-\mathbf{k}$ before collapsing into an outgoing photon with the energy ω_f (see Fig. 2). Our primary goal is to calculate the dependence of this matrix element on the incident photon frequency.

We use the spin density wave (SDW) formalism [12] to describe the electronic state at

half-filling and the excitations around it. In the SDW formalism one introduces a long-range order in $\mathbf{S}_q = \sum_k c_{k+q,\alpha}^\dagger \sigma_{\alpha,\beta} c_{k,\beta}$ with $\mathbf{q} = \mathbf{Q} \equiv (\pi, \pi)$ and uses it to decouple the Hubbard interaction term. The diagonalization then yields two bands of electronic states (the conduction and valence bands) with $E_k = \pm \sqrt{\epsilon_k^2 + \Delta^2}$, where the $2\Delta \sim U$ in the strong coupling limit that is assumed throughout this work. In terms of the conduction and valence band quasiparticle operators $a_{k\sigma}$ and $b_{k\sigma}$, the current operator is interband to leading order in t/U , $\mathbf{j}_{q=0} \Rightarrow \sum_k' \frac{\partial \epsilon_k}{\partial \mathbf{k}} (a_{k\sigma}^\dagger b_{k\sigma} + b_{k\sigma}^\dagger a_{k\sigma})$. We also need the magnon-fermion interaction. Its derivation in the SDW formalism is straightforward, as the magnons are described as collective modes in the transverse spin channel [12]. The answer is, for $S = 1/2$,

$$H_{\text{el-mag}} = \sum_{k,q}' (a_{\alpha,k}^\dagger a_{-\alpha,k+q} e_q^\dagger \Phi_{aa}(k, q) + a_{\alpha,k}^\dagger b_{-\alpha,k+q} e_q^\dagger \Phi_{ab}(k, q) + (a \rightarrow b) + \text{H.c.}) \quad (2)$$

where e_q are the magnon operators, $\eta_q, \bar{\eta}_q = \frac{1}{\sqrt{2}} \left(\frac{1 \mp \gamma_q}{1 \pm \gamma_q} \right)^{1/4}$, $\gamma_q = (\cos q_x + \cos q_y)/2$, and, to leading order in t/U , the vertex functions are given by

$$\begin{aligned} \Phi_{aa,bb}(k, q) &= \left[\pm(\epsilon_k + \epsilon_{k+q})\eta_q + (\epsilon_k - \epsilon_{k+q})\bar{\eta}_q \right]; \\ \Phi_{ab,ba}(k, q) &= 2\Delta \left[\eta_q \mp \bar{\eta}_q \right]. \end{aligned} \quad (3)$$

In the situation when the photon frequencies are much smaller than Δ all the energy denominators are of order U , and the dominant diagrams for the Raman vertex are simply those with the largest numerators. It then follows from (3) that one has to consider processes in which the fermion changes bands while emitting a magnon. A representative diagram is shown in Fig. 2a. We collected all the leading order diagrams for the Raman matrix element and obtained

$$M_R^1 = \alpha \sum_{a=x,y} e_{ia} e_{fa}^* \left[\cos q_a (\lambda_q^2 + \mu_q^2) - 2\lambda_q \mu_q \right], \quad (4)$$

where $\sqrt{2}\mu_q = \bar{\eta}_q + \eta_q$, $\sqrt{2}\lambda_q = \bar{\eta}_q - \eta_q$, and $\alpha = 16t^2\Delta/(4\Delta^2 - \omega^2)$. This is exactly the expression which Shastri and Shraiman obtained in their derivation of the Loudon-Fleury vertex for the Hubbard model. Observe that within the Loudon-Fleury model, the

scattering in the A_{1g} geometry ($\hat{\mathbf{e}}_i = \frac{\hat{\mathbf{x}}+\hat{\mathbf{y}}}{\sqrt{2}}$, $\hat{\mathbf{e}}_f = \frac{\hat{\mathbf{x}}+\hat{\mathbf{y}}}{\sqrt{2}}$), vanishes, because in the A_{1g} geometry the Loudon-Fleury and Heisenberg Hamiltonians commute with each other. On the contrary, in the B_{1g} scattering geometry ($\hat{\mathbf{e}}_i = \frac{\hat{\mathbf{x}}+\hat{\mathbf{y}}}{\sqrt{2}}$, $\hat{\mathbf{e}}_f = \frac{\hat{\mathbf{x}}-\hat{\mathbf{y}}}{\sqrt{2}}$) the Raman vertex is finite, $M_R^{B_1} \sim (\mu_q^2 + \lambda_q^2)(\cos q_x - \cos q_y) = \frac{\cos q_x - \cos q_y}{\sqrt{1-\gamma_q^2}}$. The profile of the two-magnon Raman scattering in the B_{1g} geometry, including the final state interaction between magnons, has been studied several times in the literature [3,5]. The two-magnon intensity has a narrow peak at the transferred frequency $\omega \sim 3J$.

A more careful treatment is, however, necessary in the resonant region, when the incoming photon frequency is close to the gap value, and one can no longer neglect the quasiparticle dispersion in the denominators. In fact, most of the experiments on Raman scattering have been performed in the frequency range where both ω_i and ω_f differ from U only to order J . In this situation, we found that the diagrams with the intraband fermion-magnon vertices become dominant, since they contain more resonant denominators. We analyzed these diagrams and found that the most singular contribution to the Raman vertex comes from the one in Fig. 2b. The internal frequency integration in this diagram results in

$$M_R^{(2)} = -8i \sum_k' \frac{\left(\frac{\partial \epsilon_k}{\partial \mathbf{k}} \cdot \hat{\mathbf{e}}_i\right) \left(\frac{\partial \epsilon_{k-q}}{\partial \mathbf{k}} \cdot \hat{\mathbf{e}}_f^*\right) [\mu_q \epsilon_{k-q} - \lambda_q \epsilon_k]^2}{(\omega_i - 2E_k + i\delta)(\omega_i - \Omega_q - E_k - E_{k-q} + i\delta)(\omega_f - 2E_{k-q} + i\delta)}, \quad (5)$$

where $\Omega_q = 2J\sqrt{1-\gamma_q^2}$ is the semiclassical spin-wave frequency. A study of the integral shows that there is a region of ω_i and ω_f where all three of the denominators in (5) vanish simultaneously, and the velocities $\mathbf{v}_k = \partial E_k / \partial \mathbf{k}$ and \mathbf{v}_{k-q} are antiparallel to each other (otherwise, the integral over \mathbf{k} vanishes). This phenomenon is known as a triple resonance [10,11]. Via a combination of analytical and numerical techniques, we found that for relevant ω_i the triple resonance in the Raman vertex occurs only in a narrow range of the final photon energies ω_f . The region of triple resonances is shaded in Fig. 3.

It is important for our considerations that the triple resonance in the Raman vertex occurs only if both excited magnons are on the mass shell (only then is the second denominator in (5) a half-sum of the other two). This is true only for the diagram which does not contain final-state magnon-magnon interactions. On the other hand, for $S = 1/2$, the dominant

contribution to the conventional two-magnon peak at $\sim 3J$ comes from the diagrams with magnon-magnon interactions [5]. In this situation the Raman spectrum $R(\omega)$ can be considered as containing two *independent* peaks: one is due to the triple resonance in M_R in the shaded region in Fig. 3, which for most of the experimentally measured ω_i is located close to $4J$, and the other, at transferred frequency of about $3J$, is due to the magnon-magnon scattering. Without considering in detail the effects of the fermionic damping, which smear the singularity in M_R , we cannot conclude which of the two peaks is stronger. The experiments indicate that the peak at $3J$ is stronger than that at $4J$, and the enhancement of the Raman matrix element at larger transferred frequencies is responsible for the observed asymmetric shoulder-like behavior of the two-magnon profile. Suppose we now fix ω at the two-magnon peak frequency $3J$, as in Fig. 1, and consider the variation of the peak amplitude as a function of the incident photon frequency ω_i . Obviously, this amplitude will by itself have a maximum when the two peaks in $R(\omega)$ merge, *i.e.*, when the $\omega = \text{const}$ line intersects the region of triple resonances. From Fig. 3 we see that the intersection occurs in a very narrow region of ω_i close to $\omega_i^{\text{max}} = 2\Delta + 8J$, where the particle and hole are excited near the *tops* of their respective bands [13]. We calculated Raman vertex in the vicinity of the intersection and found that it diverges (in the absence of damping) as

$$M_R \sim \frac{\omega_i^{\text{max}} - \omega_i}{(\omega_i - \omega_i^{\text{res}} + i\delta)^{3/2}}, \quad (6)$$

where ω_i^{res} can be well approximated by $\omega_i^{\text{res}} = \omega_i^{\text{max}} - (\omega - 2J)^2/8J$. The $3/2$ power of the denominator in (6) is due to triple resonance, while the small factor in the numerator comes from the vanishing of the numerator in (5) right at the top of the band (*i.e.*, at $\mathbf{k} = \mathbf{0}$). In practice, the difference between ω_i^{res} and ω_i^{max} can be neglected, and Eq. (6) yields inverse square-root singularity in M_R , which implies a linear singularity in the Raman intensity, $R \sim |M_R|^2 \sim |\omega_i - \omega_i^{\text{res}}|^{-1}$.

Eq. (6) is a key result. In essence, we have found that the intensity of the two-magnon peak increases by an inverse linear law as one approaches the upper edge of the fermionic band. We emphasize that the singularity at the top of the band exists, due to the triple

resonance effects, despite the vanishing of the numerator in (5) at this point.

We now discuss how these (and other) results are related to experiment. We listed the key experimental features in the beginning of the paper. Here we comment on each of them: (a) *asymmetry of the two-magnon peak profile*: our theory predicts that for ω smaller than ω_i^{res} the two-magnon peak profile should be asymmetric, with the “shoulder-like” behavior at frequencies close to $\omega = 4J$. This is consistent with experimental observations. In particular, the experimentally measured two-magnon profile in Pr_2CuO_4 was analysed [14] and found to contain two peaks, a two-magnon peak at $3000cm^{-1}$, and a smaller one at $4000cm^{-1}$, which is precisely as expected from our calculations; (b) *selection rules*: the leading diagram in the resonance regime contributes to the scattering in both B_{1g} and A_{1g} geometries. The signals in both geometries have been observed in the experiments. Recall that the Loudon-Fleury theory predicts scattering only in the B_{1g} geometry; (c) *a single peak*: our theory predicts a *single* maximum in the two-magnon peak intensity measured as a function of the incident photon frequency, while from the “Loudon-Fleury” diagrams we might have expected two peaks, one at $\omega_i = 2\Delta$, and the other at $\omega_f = 2\Delta$ (the incoming and outgoing resonances) [10]; (d) *peak location and shape*: our theory predicts the maximum of the two-magnon peak intensity measured as a function of ω_i right near the upper edge of the quasiparticle fermionic band. This is consistent with the measurements of the dielectric constant, which show that the Raman scattering is strongest right at the upper edge of those features in the optical data that can be interpreted as particle-hole excitations between the lower and upper fermionic bands. We fitted the data on the peak intensity from Fig. 1 by our Eq. (6) and found a satisfactory agreement with the predicted inverse linear dependence, except in the immediate vicinity of the resonance, where the effects of fermionic damping become relevant.

To summarize, we developed a diagrammatic approach to Raman scattering in antiferromagnetic insulators which can be used in both the resonant and nonresonant regimes. We described for the first time the two-magnon Raman scattering in the resonant regime, when the incident and final photon frequencies are only $\mathcal{O}(J)$, apart from the gap between

conduction and valence bands. This frequency range is relevant to recent experiments on undoped high- T_c compounds. We identified the diagram which gives a dominant contribution to the Raman vertex in this regime, and found the region in the (ω_i, ω_f) plane where the Raman vertex is strongly enhanced due to triple resonance. We demonstrated that the triple resonance, *combined with the SDW dispersion relation for the carriers*, explains the unusual experimental features in the two-magnon profile and in the two-magnon peak intensity dependence on the incoming photon frequency. In particular, our theory predicts the maximum of the two-magnon peak intensity right at the upper edge of the features in the optical data, as observed in several materials [9]. This serves as a partial verification of the SDW picture for the carriers, which, despite much theoretical work, has not been well-established experimentally in these materials.

Beyond the scope of the present theory are the unexpectedly large width of the symmetric part of the two-magnon peak, which is probably related to the magnon damping due to the interaction with phonons [15], and the existence of a considerable Raman signal $R(\omega)$ well above the maximum possible two-magnon energy (i.e., $4J$) [16], which may be related to chiral spin fluctuations [17].

It is our pleasure to thank G. Blumberg, C. Canali, S.L. Cooper, D. Khveshchenko, M.V. Klein, R. Liu, R. Martin, R. Merlin, H. Monien, D. Pines, S. Sachdev, C.M. Varma, P. Wiegmann and A. Zawadowski for useful discussions, and R. Liu and S.L. Cooper for providing the experimental data. D.F. was supported by the Texas Center for Superconductivity at the University of Houston and by the NSF Grant No. DMR 91-20000 through the Science and Technology Center for Superconductivity at the University of Illinois. Part of the work has been done while A.C. was at Yale University, where he was supported by the NSF Grants No. DMR-8857228 and DMR-9224290.

REFERENCES

* Present address.

- [1] Discussion between P.W. Anderson, D. Pines, and D.J. Scalapino, *Physics Today* **47**(2), 9 (1994); P. W. Anderson and J. R. Schrieffer, *Physics Today* **44**(6), 54 (1991); a column in *Science* **261**, 294 (1993).
- [2] M.G. Cottam and D.L. Lockwood, *Light Scattering in Magnetic Solids* (Wiley, New York, 1986).
- [3] R.R.P. Singh, *Comments Cond. Mat. Phys.* **15**, 241 (1991).
- [4] K.B. Lyons, *et. al.*, *Phys. Rev. Lett.* **60**, 732 (1988).
- [5] C.M. Canali and S.M. Girvin, *Phys. Rev. B* **45**, 7127 (1992).
- [6] P.A. Fleury and R. Loudon, *Phys. Rev.* **166**, 514 (1968).
- [7] B.S. Shastry and B.I. Shraiman, *Phys. Rev. Lett.* **65**, 1068 (1990); *Int. J. Mod. Phys. B* **5**, 365 (1991).
- [8] S. Sugai, S. Shamoto, and M. Sato, *Phys. Rev. B* **38**, 6436 (1988).
- [9] R. Liu, *et. al.*, *J. Phys. Chem. Solids* **54** 1347 (1993).
- [10] M. Cardona, in *Light Scattering in Solids II*, M. Cardona and G. Güntherodt, eds. (Springer-Verlag, New York, 1982).
- [11] R.M. Martin and L.M. Falikov, in *Light Scattering in Solids*, M. Cardona, ed. (Springer-Verlag, New York, 1975).
- [12] J.R. Schrieffer, X.G. Wen, and S.C. Zhang, *Phys. Rev. B* **39**, 11663 (1989); A.V. Chubukov and D.M. Frenkel, *Phys. Rev. B* **46**, 11884 (1992).
- [13] There is a second crossing as $\omega_i \sim 2\Delta + 2J$, but in this region only a small fraction of magnon directions, namely $q_x \approx q_y$ allow for a triple resonance.

- [14] I. Tomeno, *et. al.*, Phys. Rev. B **43**, 3009 (1991).
- [15] W.H. Weber and G.W. Ford, Phys. Rev. B **40**, 6890 (1989); S. Rosenblum, A.H. Francis, and R.Merlin, Univ. of Michigan, Ann Arbor, preprint (1993).
- [16] G. Blumberg, private communication.
- [17] D.V. Khveshchenko and P.B. Wiegmann, Phys. Rev. Lett. **73**, 500 (1994).
- [18] A.V. Chubukov and D.M. Frenkel, in preparation.

FIGURES

FIG. 1. (a) A typical Raman cross-section in $YB_2Cu_3O_6$ as a function of transferred photon frequency. A two-magnon peak is clearly seen. (b) The strength of the two-magnon peak as a function of incoming photon frequency. Also shown is the imaginary part of the dielectric constant. Data courtesy of the authors of Ref. [9].

FIG. 2. (a) A representative diagram which contributes to the Loudon-Fleury Hamiltonian at small incident frequencies. Each fermion can belong to either the valence (dashed line) or conduction (solid line) band. The emitted magnons are denoted by the solid wavy lines. (b) The most singular diagram at resonance.

FIG. 3. The triple resonance region (shaded) in the (ω_i, ω) plane where $\omega = \omega_i - \omega_f$. The horizontal line corresponds to the position of the two-magnon peak which for definiteness we chose to be at $\omega = 2.8J$ which is the value one obtains in the $1/S$ expansion neglecting the renormalization of J [18].

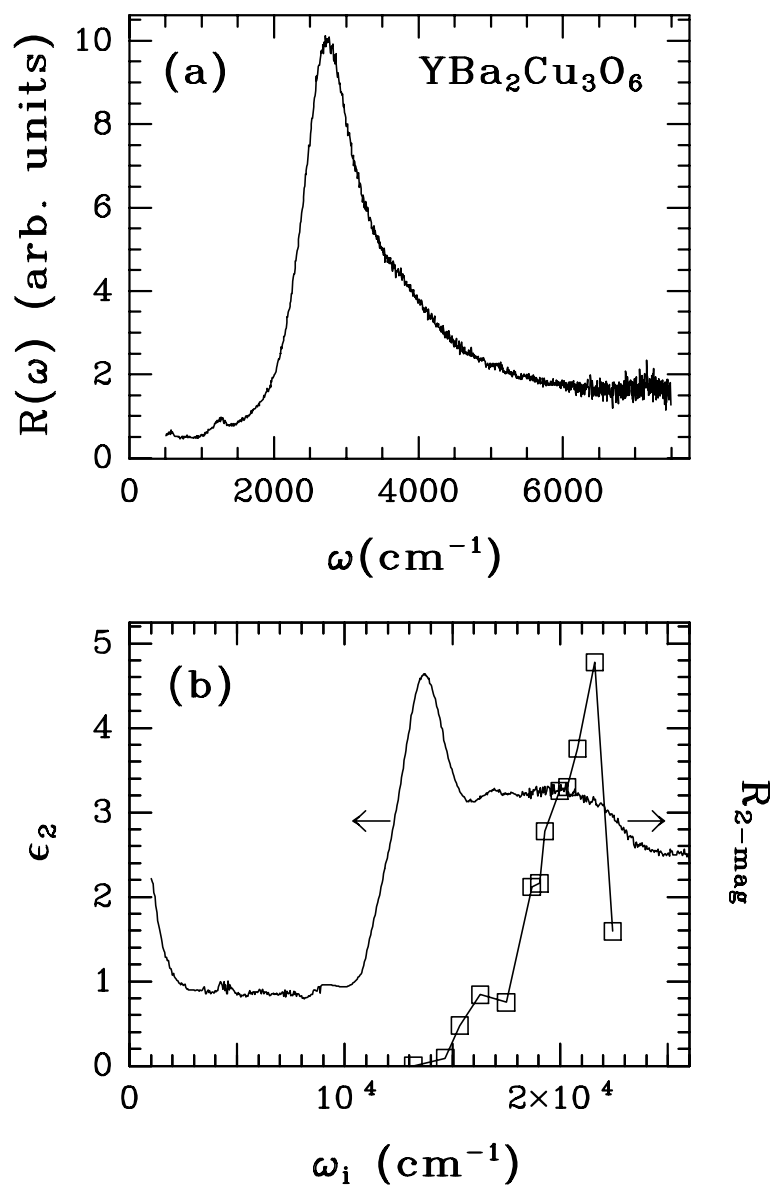


Fig. 1

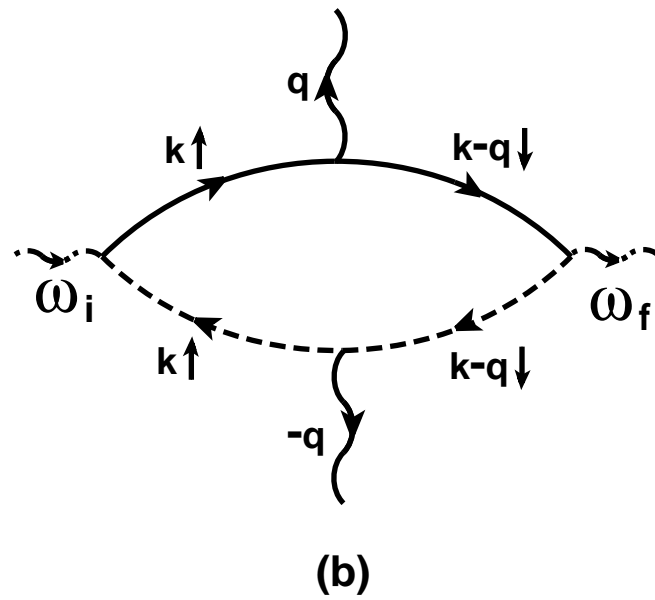
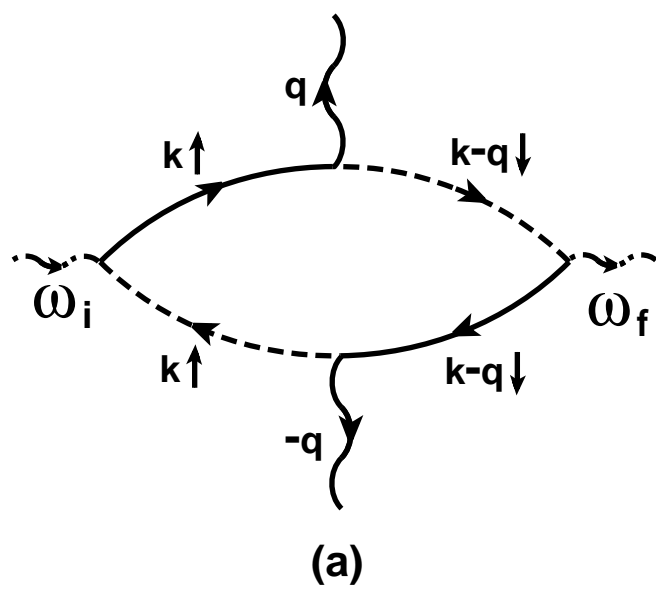


Fig. 2

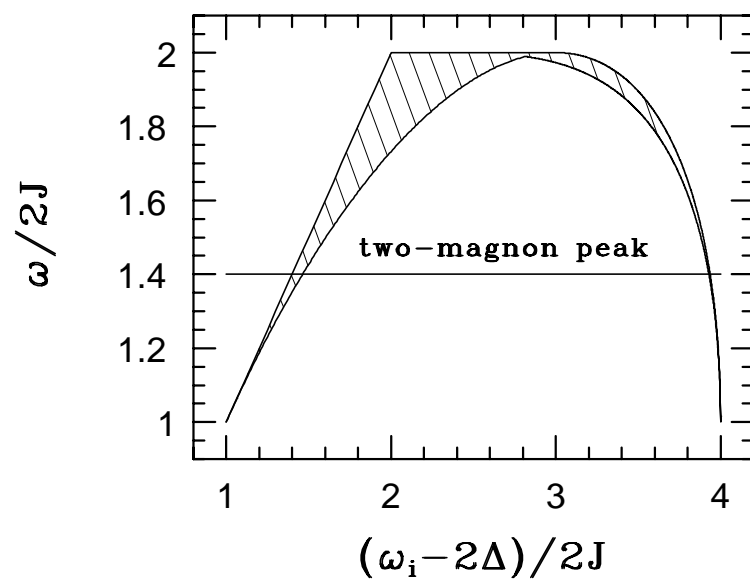


Fig. 3